ELSEVIER

Microelectronics Journal 27 (1996) 449–457
Copyright © 1996 Elsevier Science Limited
Printed in Great Britain. All rights reserved
0026-2692/96/$15.00

Research paper

0026-2692(95)00112-3

BEST PAPER AWARD ON BEHALF OF *MICROELECTRONICS JOURNAL* FOR THE CAS'94 CONFERENCE

Design of a silicon microsensor array device for gas analysis

Florin Udrea[1] and Julian W. Gardner

Department of Engineering, University of Warwick, Coventry CV4 7AL, UK

This paper describes the design of a silicon-based microsensor array for application in gas or odour monitoring. Individual sensor cells consist of both lateral and vertical electrode pairs to measure film conductance and/or capacitance. The fabrication process involves standard silicon technologies to integrate a platinum or nickel-iron heater below the sensor cells. A simulation of the device gives a thermal response time of only 60 ms and an ultra low power loss of about 50 mW at 400°C per sensor. This compares well with experimental values observed on a similar device. The process technology is suitable for both the deposition of organic materials (e.g. conducting polymers) and inorganic materials (e.g. semiconducting oxides). A scheme of the transducer interface circuitry is also provided, and could be used in a portable battery-powered instrument. Copyright © 1996 Elsevier Science Ltd.

1. Introduction

The development of an integrated silicon sensor array capable of discriminating between simple and complex odours has received considerable interest in recent years [1]. Some advantages of silicon sensors are that they offer the low power consumption necessary for portable devices, possess a fast thermal response time, can be made at low cost and permit the integration of associated electronics. Individual silicon sensor devices with a thin diaphragm featuring very low power consumption have been reported previously [2–4]. Compared with individual sensor devices a sensor array has the advantage of improved gas selectivity, lower noise and reduced effect of poisoning through superior data processing methods (e.g. adaptive neural networks).

This paper describes the theoretical design of such a microsensor array design which not only features a very low power consumption but also allows for great flexibility in the choice of the gas-sensitive material, such as low temperature organic materials (e.g. conducting polymers [5]) or high temperature semiconducting oxides [6].

[1]F. Udrea is now with the Engineering Department, University of Cambridge, Cambridge CB2 1PZ, UK.

2. Device description

2.1 Cross-section

A schematic cross-section of one cell of the silicon array device in which the active film is thermally isolated on a thin diaphragm is shown in Fig. 1. The bulk silicon is removed using an anisotropic back-etching process (e.g. KOH) to leave the thin diaphragm. The sensing cell is divided into two sensors. The first sensor comprises a pair of interdigital co-planar electrodes on top of which the sensing material is deposited, and can operate in a trans-conductive mode (termed lateral sensor). The second sensor is a sandwich structure of two electrodes and a thin gas-sensitive layer which can operate both in the capacitive and conductive mode (termed vertical sensor), thus measuring the change in the electrical conductivity and dielectric constant in the presence of gases. The integration of both geometries in the same device (i.e. lateral and vertical) gives a great flexibility in the sensor response to various gases and also helps to characterize fully the nature of the interaction between the sensing material and a given gas (e.g. reaction kinetics of the change in resistivity and dielectric constant). The heater could be placed on the surface and surround the sensitive area [7], however a vertical arrangement [2–4] as shown in Fig. 1 is preferable because it minimizes the power consumption and size of active area. The heater is sandwiched between two layers to protect it from atmospheric contamination.

2.2 Thermal losses and heater resistance

There are three main contributions to the total thermal loss: first, a thermal loss due to conduction through the diaphragm H_m; second, a loss to the surrounding air due to the thermal convection and conduction H_a; and finally a loss due to radiation H_r. The total losses are determined by the geometric size (thickness h, membrane length l and active area dimension a), the specific thermal conductivity σ of the membrane material and the temperature difference ΔT. According to Dibbern [2] the total power losses can be expressed as:

$$H_t \approx H_m + H_a \approx \left[\frac{2\pi \cdot \sigma \cdot h}{\ln(l/a)} + \alpha a^2\right]\Delta T \qquad (1)$$

where the first term is due to conduction losses while the second expresses the convection losses. For a first order approximation the radiation losses and the dependence of the convection losses with ΔT^2 at high temperatures have been neglected. In eq. (1) $\alpha \approx 0.35\,\mathrm{mW\,mm^{-2}\,K^{-1}}$, $l/a = 3$, $h = 10\,\mu\mathrm{m}$ and $\sigma \approx 2.5\,\mathrm{W\,m^{-1}\,K^{-1}}$ for glasses or oxynitrides; $h = 1\,\mu\mathrm{m}$ and $\sigma \approx 28\,\mathrm{W\,m^{-1}\,K^{-1}}$ for silicon nitride.

The heater resistance R is approximately given by:

$$R \approx \rho \frac{L}{w \cdot t} = N \cdot r \qquad (2)$$

where ρ is the resistivity of the heater material, L is the length of the heater, t is the thickness of the heater layer, w is the width of one line of heater, r is the resistance per square and N is the square number. The power P_h developed by the heater is $P_h = V_h^2/R$. For a value for P_h of 150 mW and a heater voltage V_h of 5 V the resistance should be about 165 Ω. Please note that the value of $P_h = 150\,\mathrm{mW}$ is for two sensors at 600°C which is equivalent with a power consumption of 50 mW per sensor at 400°C.

Several materials can be used to make the heater, such as polysilicon, platinum or NiFe. The material selected by Dibbern [2] was NiFe (81:19) permalloy, which offers a high stability

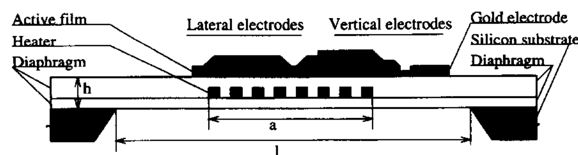

Fig. 1. Schematic cross-section of one sensing cell of a silicon microsensor array device.

against electromigration and tolerates a current density up to 10^{11} A/m^2. The specific resistivity at 600°C is about 7.5×10^{-7} Ωm. Permalloy has a significant temperature coefficient of resistance (TCR) which enables temperature measurement by the heater itself, thus eliminating the need for an additional temperature sensor. Another commonly used material for the heater is platinum. Platinum is easy to deposit and has a linear and stable TCR at high temperatures. The compromise between a relatively large sensitive area and a small active area to minimize the losses leads to a value of a of 0.5 mm (a is the dimension for the square active area, as shown in Fig. 1). It should be noted that although the resolution of microlithography permits much smaller values of a, a very small sensitive area will adversely affect the robustness of the sensor due to easier contamination. Moreover, for conducting polymers, the reduction of the electrode area is limited by the ability of the potentiostat to grow polymers reliably with minute currents [8]. For $a = 0.5$ mm from eq. (1), one can obtain the total thermal losses in the device: $H_t = 135$ mW at 600°C. The electric power will be slightly greater than the estimated thermal losses. This is the reason that we have already chosen $P_h = 150$ mW. The shape of the heater is given in Fig. 2 (top). There are three basic requirements for the heater geometrical design: first, that the heater electrode should cover uniformly the sensing area (to avoid any gradients in the temperature); second, that the heater resistance is higher enough at those dimensions to provide a driving voltage to be about 5 V at the required operating temperature; and third, that the heater dimensions should be small (heater area, heater thickness) to reduce the radiation losses. The following dimensions for the heater have been chosen for our particular design and in accordance with our laboratory facilities [9]: width of the heater truck $w = 40\,\mu$m, length of the heater truck $L = 480\,\mu$m, the gap between two trucks $g = 25\,\mu$m, number of trucks $n = 8$ and the thickness of the heater layer $t = 0.5\,\mu$m. The square resistance has been evaluated at $r = 1.5\,\Omega$ per square, and the numbers of squares $N \approx 100$.

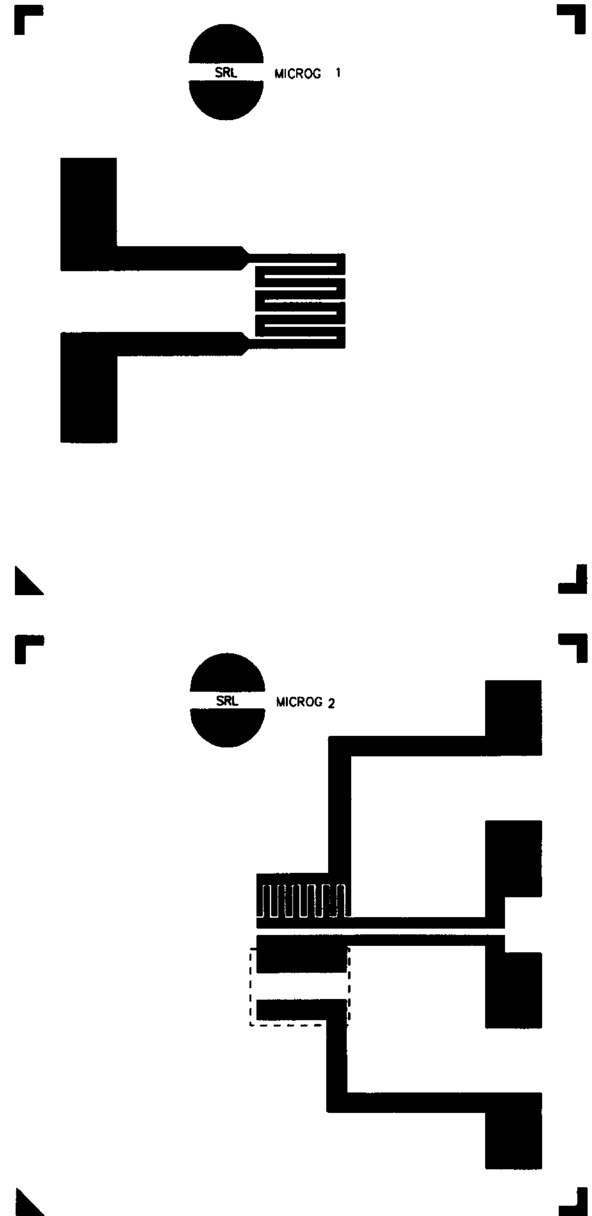

Fig. 2. Mask patterns for the cell heater (top) and sensing electrodes (bottom). The top electrode location is represented by a dotted line.

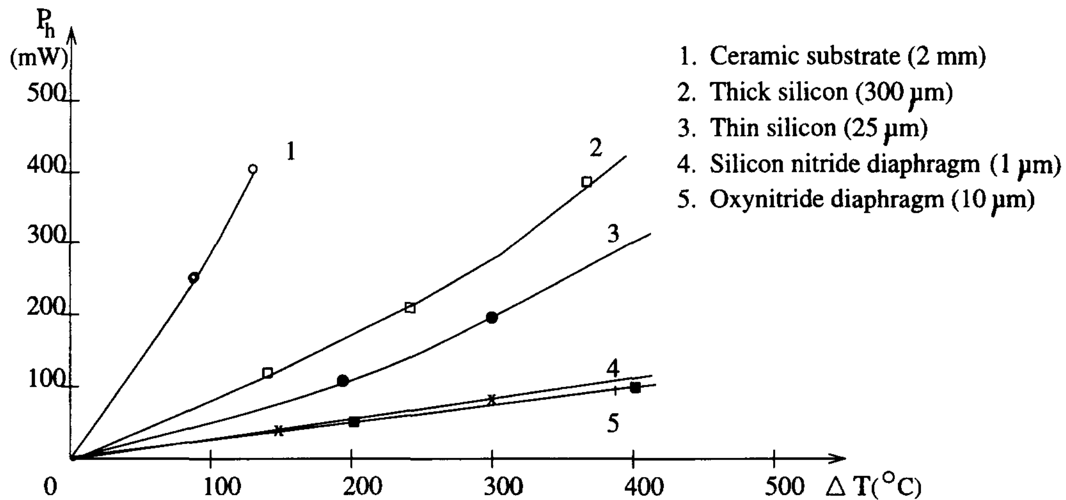

Fig. 3. Theoretical heater power consumption for oxynitride and silicon nitride membranes and test measurements for ceramic thick silicon and thin silicon substrates from [10].

Figure 3 shows the theoretical heater power consumption P_h against the operating temperature relative to ambient, ΔT. The theoretical power losses estimated for the oxynitride and silicon nitride membranes are considerably lower than the experimental values reported for ceramic, thick silicon and thin silicon [10].

A two-dimensional numerical simulation using the simulator TMA MEDICI [11] of the lattice temperature distribution in the sensor cell was performed. The bridge structure shown in Fig. 1 was imported in MEDICI and simulated using a non-uniform grid with high density in the diaphragm area. The lattice heat equation available in MEDICI accounts for the conduction losses in the diaphragm and outside the diaphragm frame. Simulations have been performed on both silicon nitride diaphragm (thickness $= 1\,\mu m$) and oxynitride (thickness $= 10\,\mu m$). The results (Fig. 4) show that the temperature is uniformly distributed in the active area and decreases abruptly outside the diaphragm area. This is consistent with the temperature measurements of the silicon substrate and diaphragm reported by

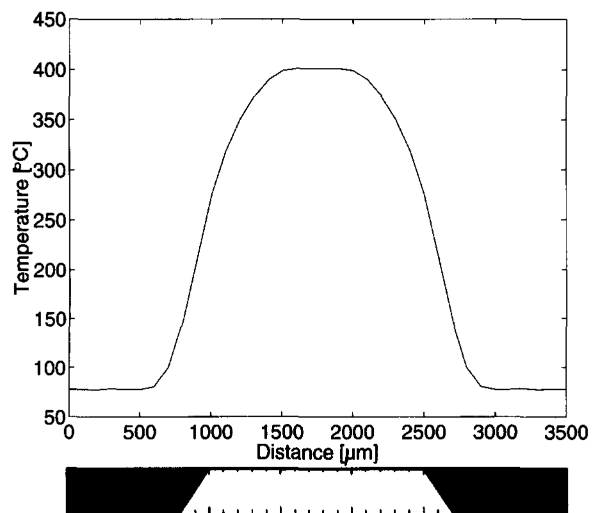

Fig. 4. Theoretical temperature distribution in the cross-section of the sensor cell. The power consumption in this case is nominally 100 mW per cell (50 mW per sensor). Data extracted from numerical simulations using MEDICI.

Krebs and Grisel [4]. Low temperatures outside the diaphragm area suggest that theoretically it is possible to integrate an electronic transducer in the same chip with the sensing device.

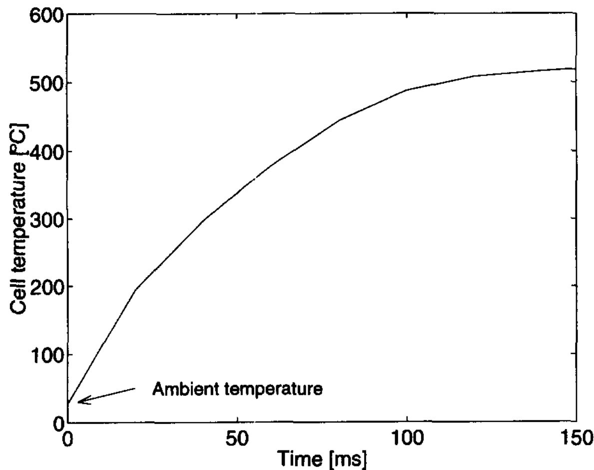

Fig. 5. Thermal response of the diaphragm of the sensor cell. The heater driving voltage rises from 0 to 4 V in 1 μs.

The thermal response time to a rise in the electric voltage applied across the heater electrodes determines the maximum rate at which temperature cycles can be run. It was mentioned that one of the advantages of the silicon sensors is their fast thermal response. In Fig. 5 a numerical simulation of the thermal response for an increase in the heater voltage from 0 to 4 V in 1 μs is shown. The thermal response time is very low and has a value of around 60 ms.

2.3 The base-line resistance of the sensitive element

The base-line resistance is defined as the resistance in air under ambient conditions. For the vertical structure, the capacitance C_{01} and the resistance R_{01} are given by:

$$C_{01} = \frac{\varepsilon_1 S_1}{h_1}; \quad R_{01} = \frac{\rho_1 h_1}{S_1} \tag{3}$$

where ρ_1, ε_1, h_1 and S_1 are the resistivity, the dielectric constant, the thickness and the area of the sensing material, respectively. For the lateral sensor, the base-line resistance is written as [9]:

$$R_{02} = \frac{\pi \cdot \rho_2}{l_2} \cdot \frac{1}{\ln\left(\frac{2h_2}{w_2} + \sqrt{\left(\frac{2h_2}{w_2}\right)^2 + 1}\right)} \tag{4}$$

where ρ_2 and h_2 are the resistivity and the thickness of the planar cell sensing material respectively, l_2 is the total length of one electrode and w_2 is the gap between electrodes. For the design shown in Fig. 2 (bottom), $h_1 = 1\,\mu$m, $S_1 = 480\,\mu\text{m} \times 160\,\mu$m, $h_2 = 1\,\mu$m, $w_2 = 15\,\mu$m, $l_2 = 2.4$ mm. ρ_1 and ρ_2 vary for various sensing materials (metal oxides, polymers) between 10^{-2} and $10^3\,\Omega$m.

3. Fabrication process

The technological process proposed for the fabrication of these devices uses eight photographic masks. In the case of tin oxide deposition: Mask1 — photolithographic patterning of the heater (Fig. 2 top); Mask2 — photolithographic patterning of the sensing element electrodes (Fig. 2 bottom); Mask3 — tin oxide deposition; Mask4 — top porous thin electrode deposition (in the sandwich cell), Mask5 — diaphragm formation, anisotropic back etching of silicon using a silicon oxide layer as a stop and KOH as etchant; Mask6 — photolithographic opening of windows in diaphragm material (in the outer frame) to form contacts with the top electrodes; Mask 7 — photolithographic opening of windows in diaphragm material (in the outer frame) to form contacts with the bottom heater layer; Mask8 — to increase the metal thickness in the pad zones. For more details of a possible fabrication process see [12].

For polymer films that react with gases at temperatures less than 120°C, a simplified process using only five masks (masks 3, 5 and 7 are removed) can be employed. Although the use of polymers as the active material reduces the number of masks and eliminates the need for a thin suspended diaphragm structure, special

deposition equipment is needed to grow the polymer on chip [8]. Presently, polymer research is being directed towards the control of the electrical properties of conductive polymers, in particular the base-line resistivity, the drift in time, and temperature [13].

3.1 Diaphragm film deposition

The most important part of a silicon array device which is required to operate at high temperature is the diaphragm. The material and method of deposition determine clearly the mechanical stability, stress and low power consumption of the diaphragm. Oxynitrides or a sandwich combination between plasma oxide and plasma nitride (to compensate for the stresses) seem to match our requirements [2]. Another solution is to use boron silicate glasses which offer a very low specific conductivity [9]. The thickness of the diaphragm is chosen to be $h = 10\,\mu$m, oxynitride, which results in power losses of only 50 mW per sensor at 400°C. If the mechanical problems can be overcome (e.g. by reducing the intrinsic stress during deposition) the thickness of the diaphragm can be reduced and thus silicon nitride (low-stress LPCVD deposition [12]) or amorphous carbon-type materials could be used. However, it is important to note that the thermal conductivity of silicon oxides is an order of magnitude lower than that of silicon nitrides, therefore in order to obtain a good thermal insulation, very thin diaphragms are required (e.g. less than 1 μm).

4. Transducer and interface circuitry

A block scheme of the interface circuitry and the transducer is shown in Fig. 6. The transducer comprises two basic circuits, a 'delta' circuit designated to give a linear output response with the change in conductance ($\delta = (G_x - G)/G_0 = R_x/(R_0 - R_x)$, where G_0 and R_0 are the base-line conductance and resistance) and a bridge circuit which can measure both the change in resistance and capacitance due to the presence of gases. The basic diagrams of the delta and bridge circuits are shown in Fig. 7. In the case of the delta circuit, the drift of the base-line resistance is compensated by adjusting the resistance R_0 so that the output voltage is virtually equal to zero. The output voltage which is linearly proportional with the change in the conductance due to the presence of gases can be amplified using the feedback resistance of the second operational amplifier, R_2.

$$\delta = \frac{R_0}{R_2} \frac{V_0}{V_{\mathrm{REF}}} \tag{5}$$

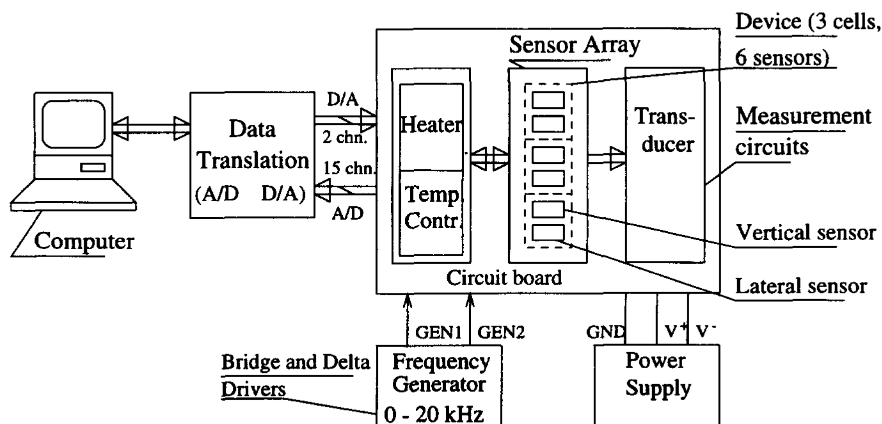

Fig. 6. Schematic diagram of the transducer and interface circuitry.

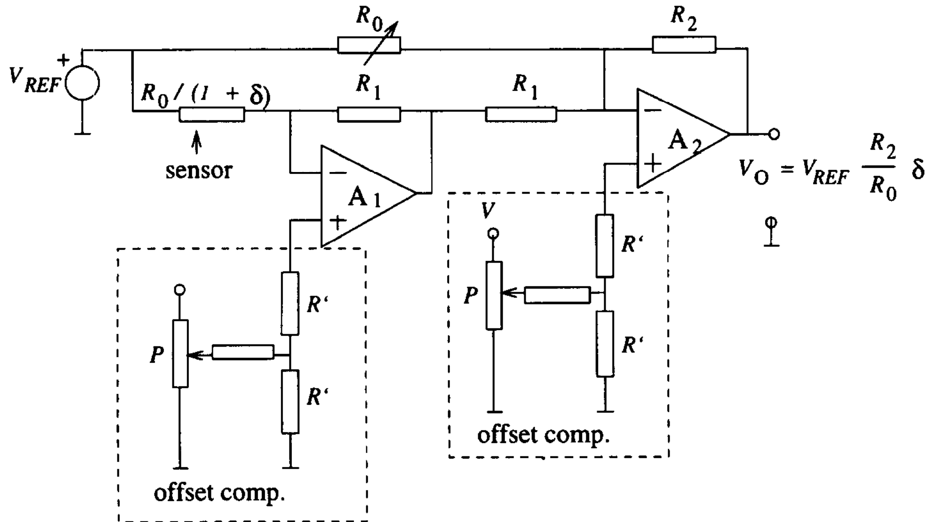

a)

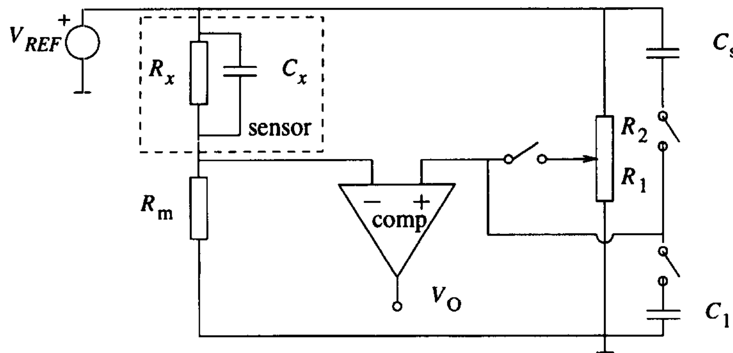

b)

Fig. 7. Schematic electrical diagrams of (a) the delta circuit and (b) the bridge circuit.

In the case of the bridge circuit, the base-line resistance drift is eliminated by balancing the bridge in clean air. The change in the resistance is then given by:

$$\delta = \frac{1}{\beta} \cdot \frac{V_0}{(\beta - 1)V_{\mathrm{REF}} - V_0} \tag{6}$$

where $\beta = R_1/(R_1 + R_2) = R_m/(R_0 + R_m)$.

The absolute value of the capacitance in the presence of gases can be obtained by using step by step measurement to separate the sensor resistive component. Initially the bridge is balanced at low frequency from R_1 and R_2 and at high frequency from C_s with C_1 disconnected. Subsequently, connecting C_1 and disconnecting the potentiometer $R_{1,2}$ one can find out the value of the sensor capacitance C_x as:

$$C_x \simeq \frac{R_1 C_1}{R_m} \frac{V_0}{V_{\text{REF}} - V_0} \quad (7)$$

and the change in capacitance as: $\delta_c = (C_x - C_0)/C_0$.

A driving circuit for the heater and a temperature controller integrated with the computer are shown schematically in Fig. 6. The driving circuit consists of a constant current source which receives the input data from the computer. The temperature is measured by detecting the variation of the heater resistance and can be accurately adjusted through a high speed 12-bit ADC card (e.g. Data Translation DT 2811).

5. Results and further work

Figure 8 shows a photograph of the prototype silicon device fabricated at Warwick University in 1992 [9] consisting of three sensor cells each with lateral and vertical sensing electrodes. The structure permits the simultaneous measurement of film conductance and capacitance in different directions. For this particular device polypyrrole was used as a sensitive material. The polypyrrole layer was grown onto the electrical electrodes using a new electro-chemical method [8]. A set of more advanced fabricated silicon sensor array devices is shown in Figs. 9a and 9b.

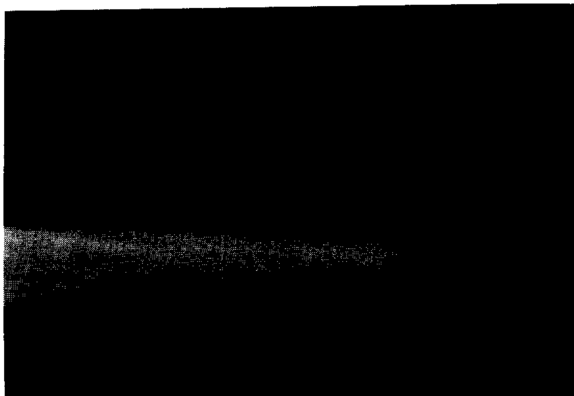

Fig. 8. A prototype silicon sensor array device for gas analysis.

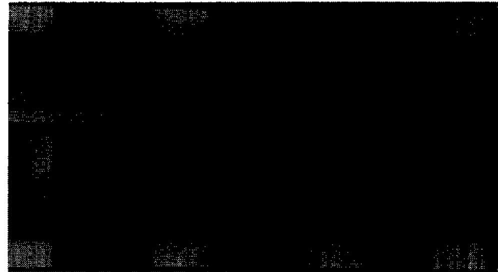

(a)

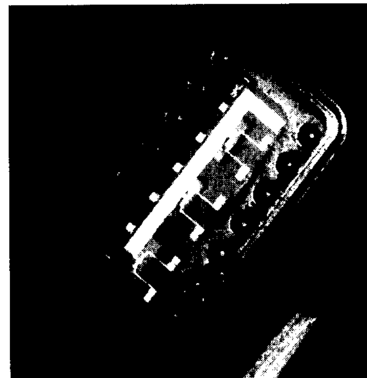

(b)

Fig. 9. Photographs of (a) the cell structure of a 0.5 μm Si_3N_4 diaphragm with integrated platinum heater and interdigitated electrodes and (b) the array device mounted on a 14 pin 0.1 inch d.i.l. package [12]. The large truck shows a common for the six sensor inputs. The three heaters are not commoned.

These devices are comprised of six sensors (two per cell) with an ultra thin Si_3N_4 diaphragm deposited by a low stress LPCVD technique at the University of Neuchatel [12]. The experimental results of the power losses per sensor agree well with the theoretical predictions (Fig. 10). Full experimental results on these sensor array devices, which include measurements of the time constants and the sensor response to various solvents such as toluene, *n*-propanol, methanol, etc. have been reported elsewhere [12]. The measurements presented in [12] discuss doped tin oxide as the sensing material. Work on sensor arrays using polymers and sensor arrays with mixed conductive polymers

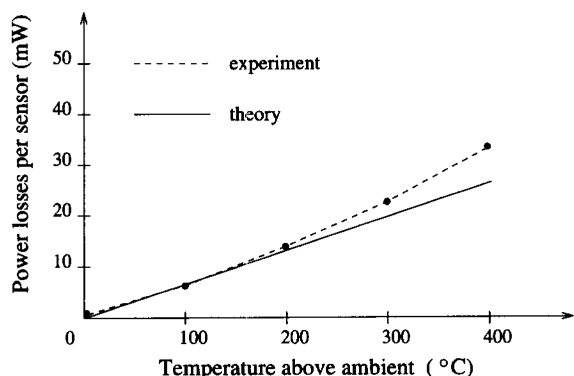

Fig. 10. Theoretical and experimental results of power losses per sensor. The dotted line shows the actual behaviour of a Si_3N_4 array device with a ultra thin diaphragm of 500 nm (from [12]).

and semiconducting oxides is presently under way in the Sensors Research Laboratory, University of Warwick, and will be reported soon.

6. Conclusions

This paper describes the design of a silicon microsensor array device suitable for application in gas or odour monitoring. The theoretical values of the heater resistance, cell power consumption and thermal response agree well with experimental values. The ultra low power consumption of about 50 mW per sensor at 400°C and ultra fast thermal response time of about 60 ms make this an attractive device for practical use. For example, the device temperature could be modulated sinusoidally, to obtain rapidly the characteristic response-temperature curve for target gases. Dynamic models could then be used to enhance the specificity of this device over conventional gas sensors which operate at a constant temperature. Moreover, an array with some replicated sensors could be used to reduce noise and remove common-mode effects in bridge arrangements [14].

Acknowledgement

The authors wish to thank the European Tempus Office for the financial support of F. Udrea. The authors also thank Colin Bidmead for help in fabricating the Warwick devices, and both Tsung Tan and Timothy Pearce (Warwick University) for valuable discussions.

References

[1] J.W. Gardner and P.N. Bartlett (eds.), *Sensors and Sensory Systems for an Electronic Nose, NATO ASI Series*, Kluwer Academic, Dordrecht, 1992, 327 pp.

[2] U. Dibbern, A substrate for thin-film gas sensor in microelectronic technology, *Sensors and Actuators B*, 2 (1990) 63–70.

[3] V. Demarne and A. Grisel, An integrated low-power thin-film CO gas sensor on silicon, *Sensors and Actuators B*, 4 (1991) 539–543.

[4] P. Krebs and A. Grisel, A low power integrated catalytic gas sensor, *Sensors and Actuators B*, 13–14 (1993) 155–158.

[5] P.N. Bartlett and S.K. Ling-Chung, Conducting polymer gas sensors, *Sensors and Actuators*, 19 (1989) 141–150.

[6] K. Ikohura and J. Watson, *The Stannic Oxide Gas Sensor*, CRC Press, Boca Raton, Florida, 1994, 187 pp.

[7] J.W. Gardner, H.V. Shurmer and P. Corcoran, Integrated tin oxide odour sensors, *Sensors and Actuators B*, 4 (1991) 117–121.

[8] P.N. Bartlett and J.W. Gardner, Microsensor deposition device, *British Patent Application No. 9400855.4*, 18 January 1994.

[9] F. Udrea, Design of an integrated silicon microsensor array for gas analysis. *Master of Science Thesis*, University of Warwick, August 1992.

[10] I. Stoev and D. Kohl, An integrated gas sensor on silicon substrate with sensitive SnO_x layer, *Sensors and Actuators B*, 2 (1990) 233–236.

[11] *MEDICI Manual*, Version 2.0, Technology Modeling Associates, September 1994.

[12] J.W. Gardner, A. Pike, N.F. de Rooij, M. Koudelka-Hep, P.A. Clerc, A. Hierleman and W. Gopel, Integrated array sensor for detecting organic solvents, *Sensors and Actuators B*, 26–27 (1995) 135–139.

[13] N. Blair, *Ph.D. Thesis*, Development of electrochemically produced conducting polymers for use in an electronic nose system. University of Southampton, 1994.

[14] J.W. Gardner, *Microsensors: Principles and Applications*, J. Wiley and Sons, Chichester, 1994, Chapter 12.